

The Eurasia Proceedings of Science, Technology, Engineering & Mathematics (EPSTEM), 2024

Volume 28, Pages 47-55

ICBASET 2024: International Conference on Basic Sciences, Engineering and Technology

Effect of Graphene Nanoplatelets and Accelerated Weathering on the Mechanical and Shape Memory Behaviour of 3D Printed Components

Mohamad Alsaadi

University of Limerick
Technological University of the Shannon

Eoin P. Hinchy

University of Limerick

Conor T. McCarthy

University of Limerick

Declan M. Devine

Technological University of the Shannon

Abstract: The need for sustainable materials has increased the adoption of 3D printing techniques in various applications due to their valuable advantages of obtaining complex design, fast site production, with significantly less waste, and thus more cost-effective, compared to traditional polymer processing techniques like moulding and extrusion. The objective of this work is to investigate the effect of functionalised graphene nanoplatelets and accelerated weathering ageing on the tensile, Izod impact, fracture toughness and shape memory behaviour of 3D printed methacrylate-based resin. The accelerated weathering aging of 1000 hrs was conducted on the 3D printed samples. The fracture toughness results in terms of critical stress intensity factor were calculated using single-edge notch bending (SENB) tests. The shape memory (SM) behaviour in terms of shape fixity and shape recovery results were determined using dynamic mechanical analysis (DMA). The results showed good resistance to weathering ageing and enhancement by incorporating functionalised graphene nanoplatelets. The maximum increment values of the tensile strength, impact resistance and critical stress intensity factor were 18%, 25% and 16%, respectively. The glass transition temperature values were slightly increased. The shape fixity ratios and the shape recovery ratios were greater than 97% and 90%, respectively. This study provides new knowledge in expanding and developing 4DPg in various industrial applications like in soft robotics as actuators and thermal sensors.

Keywords: 3D printing, Graphene nanoplatelets, Accelerated weathering,

Introduction

Due to several benefits from this smart fabrication method like complex design, easy access, less lead time, lower energy consumption, lower material waste and lower cost. These advantages make 3D printing (3DPg) technology a significant aspect of Industry 4.0 and a leading technique for various sectors. Additionally, these sustainable fabrication methods like liquid-based, powder-based and filament-based 3DPg have inspired and motivated the public to be employed in different uses such as education purposes, art, decoration, creating spare parts at home, and many other applications (Alsaadi et al., 2023; Mahmood et al., 2023; Prashar et al., 2022). The 4DPg manufacturing employs a smart material to fabricate a 3DPd structure that can change shape over time in response to an external stimulus. Therefore, 4DPg can play a vital role in several sustainable applications like soft robotics, energy harvesters, renewable energies, and self-healing structures (Pisani et al.,

- This is an Open Access article distributed under the terms of the Creative Commons Attribution-Noncommercial 4.0 Unported License, permitting all non-commercial use, distribution, and reproduction in any medium, provided the original work is properly cited.

- Selection and peer-review under responsibility of the Organizing Committee of the Conference

© 2024 Published by ISRES Publishing: www.isres.org

2022; Vatanparast et al., 2023). The sequences of changing shapes can be achieved for various composite structures and designs that have the SM property (Mao et al., 2015; Yu et al., 2015). For instance, Mao et al. (Mao et al., 2015) employed thermal stimulus for the 3D printed (3DPd) UV-cured epoxy-based SM polymers to achieve self-closing devices. By identifying material structure in various sections, the authors proved that the programmed component can be returned to the permanent shape in a predefined sequence, thus exhibiting a multiple-way SM polymer.

Polymeric materials can be sensitive to UV-light radiation, humidity and heat. For instance, the thermal and mechanical behaviour can be changed due to absorbing moisture, especially at high temperatures hence the water absorption into the polymer matrix can be increased (Afshar et al., 2016; Afshar & Wood, 2020). Exposure to sunlight for long intervals can initiate chain crosslinking and chain scission that can deteriorate the matrix polymeric materials by affecting their chemical compound. Chain crosslinking can make the polymer brittle, which may generate microcracks in the material surface. Chain scission may decrease the molecular weight and degrade the thermal and strength resistance of the polymer matrix (Afshar et al., 2019; Alfaro et al., 2022). Nevertheless, mechanical and thermal behaviour can be improved by short-term exposure to UV radiation, temperature and humidity (AWRTH) (Alfaro et al., 2022). For example, Golhin et al. (Golhin et al., 2023) indicated that the stiffness and T_g of the 3DPd polymer resin using a rotary PolyJet printer were improved after 58 days of AWRTH ageing due to the chain rearrangement of the liquid resin leading to denser liquid resin chains, generating more resistance for the deformation. The storage modulus can be enhanced with AWRTH ageing due to the increase of polymeric chain packing and rigidity (Spiridon et al., 2018). Bass et al. (Bass et al., 2016) reported the ultimate tensile stress and the elongation of liquid-based 3DPd resin increased over time while lighting conditions did not affect material properties significantly. On the other hand, noncovalent functionalisation by melamine has been utilized to improve nanoparticle dispersion and prevent agglomeration defects (Alsaadi et al., 2023; Shen et al., 2016; Wu et al., 2020). For instance, 4DPg of 0.1 to 0.3 wt% graphene nanoparticles reinforced acrylate resin marginally improved the T_g and tensile strength. The authors suggested that using graphene nanocomposite resins can enhance printability and create novel SM nanocomposites (Chowdhury et al., 2021).

In this experimental investigation, a DLP 3DPd resin was used to manufacture mGNP nanocomposite objects. The mechanical and fracture properties were investigated by tensile, Izod impact and single-edge notch bending tests. The fracture surface morphology of the SENB specimens was observed via scanning electron microscopy (SEM). The curing level was investigated via differential scanning calorimetry (DSC), chemical behaviour was tested via Fourier transform infrared spectroscopy (FTIR) and the SM properties via dynamic mechanical analysis (DMA).

Materials and Methods

Materials and Preparation of 3DPd Specimens

The commercial 3DPd resin used was Tough-Blk-20 resin (referred here as TG0) (3D Systems, Inc., Rock Hill, South Carolina, USA) consists of Methacrylate Ester Monomer (25-35%), Trimethyl cyclohexyl acrylate (10-20%), Isobomyl acrylate (10-20%), 2-Propenoic acid, 2-phenoxyethyl ester (1-2.5%), phenylbis (2,4,6-trimethylbenzoyl) phosphine oxide (BAPO) (1-5%) and stabiliser (1-2.5%). The GNP was used with 5 μm particle size, 15 nm thickness and $0.03\text{--}0.1\text{ g}\cdot\text{cm}^{-3}$ bulk density. Melamine was used to functionalise GNP. N,N-dimethylformamide (DMF) was used for dissolving melamine and GNP. DMF is a unique organic material with the formula $(\text{CH}_3)_2\text{NC}(\text{O})\text{H}$. It is something not only a solvent, but it can also play a significant role in organic chemistry. It can be employed as a catalyst, reagent, and stabilizer (Heravi et al., 2018). The materials were supplied by Sigma-Aldrich (Dorset, UK). TG0 resin can be used to produce 3DPd durable components (black like ABS (Acrylonitrile Butadiene Styrene)) with high UV, thermal, moisture, colour and dimension stability, which can be used for various applications like automotive styling components, consumer electronics parts, bezels, knobs, brackets, covers and robust functional prototypes (3D Systems Inc, n.d.).

The melamine was mixed with a magnetic stirrer with GNP within DMF solution followed by an ultrasonication process. As seen in Figure 1, ball-milling is used for 24 h to trigger the functionalisation process between melamine and GNP (mGNP). The melamine's hexagonal ring generates $\pi\text{--}\pi$ interactions on the GNP surface due to the ball-milling process. The mixture was vacuum filtered and vacuum dried to produce the black solid mGNP. The mGNP was examined and proved via several characterisation techniques like thermogravimetric analysis (TGA), FTIR, ultraviolet-visible (UV-Vis) spectroscopy and Raman spectroscopy (Alsaadi et al., 2023). TG0 was blended with 0.08 wt% of the mGNP at 35 °C.

The blend was stirred for 30 min and mixed for another 30 min at 1500 rpm in a planetary centrifugal mixer. Then, the prepared resin was mixed under vacuum for 20 min at 200 rpm to remove the air bubbles (Figure 1). The 3DPg process was conducted by transferring the resin to the tank of the Figure 4® printer (3D Systems, Inc., Rock Hill, South Carolina, USA). The printer's UV light is 405 nm wavelength, and the layer thickness is selected with a size of 0.1 mm. After support structure removal, the 3DPd specimens (Figure 2) were washed for 1 min by isopropyl alcohol (IPA) and UV post-cured for 90 min.

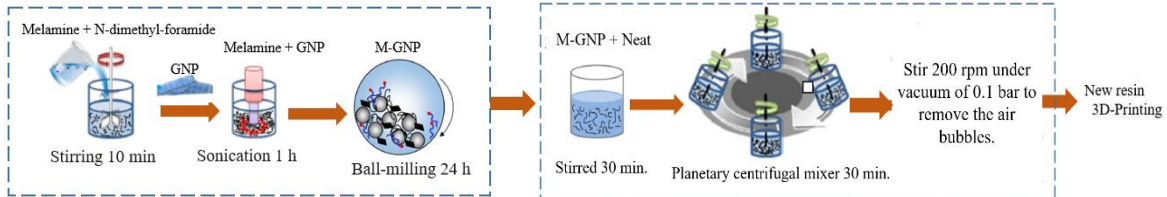


Figure 1. Schematic illustration of Ball-milling process to functionalise GNP by melamine.

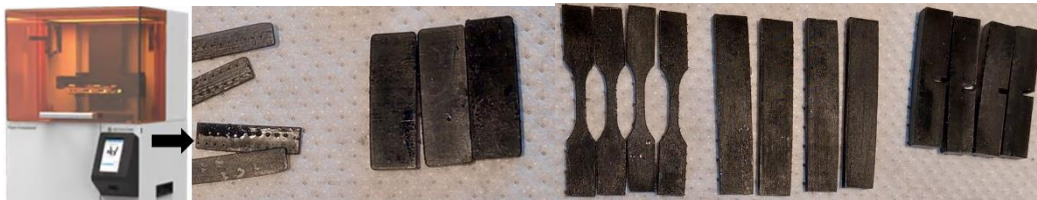


Figure 2. Figure 4® printer and 3DPd specimens.

Testing Methods

Zwick Roell machine (Z010, GmbH & Co. KG, DEU) was used for tensile experiments (gauge length of 7.62 mm) with a crosshead speed of $1 \text{ mm} \cdot \text{min}^{-1}$ according to ASTM D638 (Figure 3). The Izod impact test was carried out on an Izod impact machine (Instron CEAST) with a 5.5 J hammer according to the ASTM D4812 standard for unnotched specimens (Figure 3). The fracture toughness behaviour was investigated using a Zwick Roell machine by calculating the stress intensity factor of the SENB specimens according to the ASTM standard D5045-99 (Figure 3). The pre-crack was introduced in the 3DPg process. The crosshead speed was $2 \text{ mm} \cdot \text{min}^{-1}$. The SENB specimens were printed with a size of $52.80 \times 12.00 \times 6.35 \text{ mm}^3$. The fracture surfaces of the failed SENB specimens were investigated using Mira SEM (Tescan, Oxford Instruments, Cambridge, UK). At least four specimens were experimented for each test.

The DSC analysis was conducted using Perkin Elmer machine DSC 4000 (Norwalk, CT, USA). 7 mg samples were analysed. These were heated from 0 to $225 \text{ }^\circ\text{C}$ at $5 \text{ }^\circ\text{C}/\text{min}$, then cooled to $0 \text{ }^\circ\text{C}$ at $5 \text{ }^\circ\text{C}/\text{min}$. The DSC measurements were achieved under the nitrogen atmosphere. The FTIR test was conducted by ATR-FTIR Perkin Elmer machine (Norwalk, CT, USA) with average scan from 400 cm^{-1} to 4000 cm^{-1} wavenumber and resolution of 4 cm^{-1} .



Figure 3. Specimens under tensile, Impact and SENB tests

The SM cycling tests are conducted to characterise the SM performance in terms of shape fixity and shape recovery under DMA single cantilever mode. This technique is commonly employed for analysing the programming/recovery behaviour of SM polymers. T_g was considered as a reference temperature to design the thermomechanical SM cyclic test. The procedure is performed as follows: (1) The specimen is heated to around $15 \text{ }^\circ\text{C}$ above T_g at a rate of $5 \text{ }^\circ\text{C} \text{ min}^{-1}$ and isothermal for 20 min, (2) the specimen is deformed by applying a

force ramped at the rate of 0.5 N min^{-1} up to 3 N, (3) the specimen is cooled down to $-10 \text{ }^\circ\text{C}$ with holding the force constant, (4) the force is released (Calculate the shape fixity is at end of this step), (5) The specimen is heated back above T_g (Calculate the shape recovery is at end of this step). The procedure was repeated from step (2) to take an average of five cycles.

Results and Discussion

Tensile and Impact Behaviour

The tensile strength and elastic modulus results of the 3DPd specimens are presented in Figure 4 (a). As seen in this figure, the UV-resist DLP 3DPd polymer with its mGNP nanocomposites exhibited good mechanical results. Hence, the tensile strength and elastic modulus values improved by 18% including mGNP and slightly increased by 2% to 4 % with the AWRTH ageing. The elastic modulus values were also enhanced with the addition of mGNP with the AWRTH ageing. The Izod impact resistance values (Figure 4 (b)) were enhanced by 25% and were slightly increased with AWRTH ageing. The π - π interactions between GNP and melamine resulted in enhanced load transfer across the interface between the 3DPd matrix and GNP nanoparticle within the polymer nanocomposite (Cha et al., 2019). On the other hand, It can be presumed that, through short-term ageing, further post-curing may be initiated owing to the combined exposure influence of UV-light, temperature and humidity generating an advance action in the polymeric chains such as rearrangement, residual crosslinking and rigidity (Golhin et al., 2023).

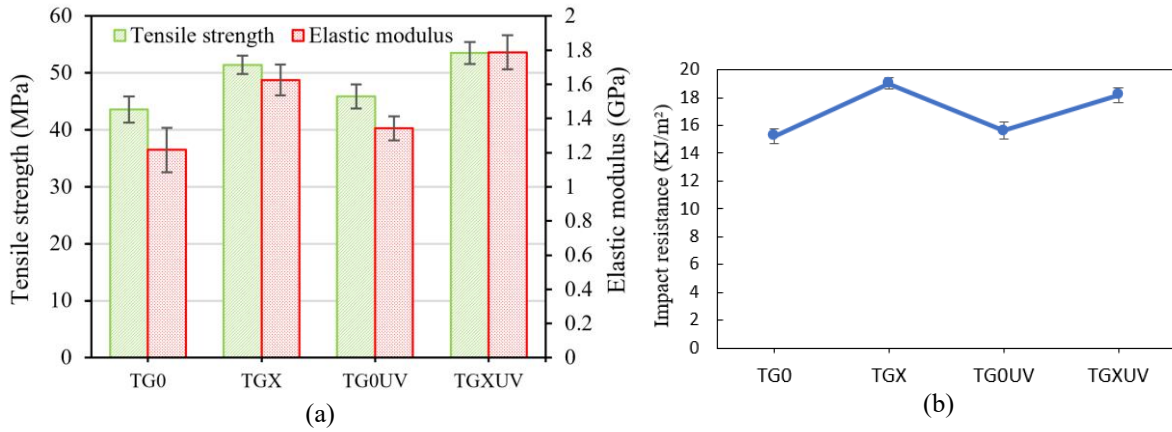


Figure 4. (a) Tensile strength and elastic modulus, and (b) impact resistance of the 3DPd specimens.

Fracture Toughness Behaviour

Fracture toughness mode I properties were determined in terms of stress intensity factor values (K_A) by testing SENB specimens. The crack length (a) was selected such that the $\frac{a}{W}$ the ratio was approximately 0.45 (W is the specimen width). The K_A values were determined as follows (ASTM D5045-99):

$$K_A = \left(\frac{P}{BW^{\frac{3}{2}}} \right) f \left(\frac{a}{W} \right) \quad (1)$$

$$f \left(\frac{a}{W} \right) = \frac{3sA^{1/2} \cdot 1.99 - A(1 - A)(2.15 - 3.93A + 2.7A^2)}{(1 + 2A)(1 - A)^{\frac{3}{2}}} \quad (2)$$

Where $A = \frac{a}{W}$, P is the fracture load, B is the specimen thickness and $f \left(\frac{a}{W} \right)$ is the correction parameter.

Figure 5 presented the stress intensity factor values of the SENB specimens. As shown in this figure, K_A values were improved by incorporating mGNP of 0.08wt% by 16%. Hence, the strong bonding between mGNP and the 3DPd resin led GNP to pin the crack front and add additional crack growth resistance, indicating an enhancement in the fracture toughness result. The K_A values were slightly increased by 1% to 3 % with the

AWRTH ageing. Figure 6 shows images for the failed SENB specimens and the fractured surfaces. The morphology of the surfaces of the failed SENB TG0 and TGX samples was observed via SEM (Figure 7). The M-GNP nanoparticles were embedded and homogeneously dispersed within the matrix. This indicates that melamine inhibits the GNP from aggregating through π - π interactions between the surfaces of GNP. Furthermore, the melamine's amino groups (-NH₂) likely bonded covalently and led to strong interfacial interactions with the polymer matrix system.

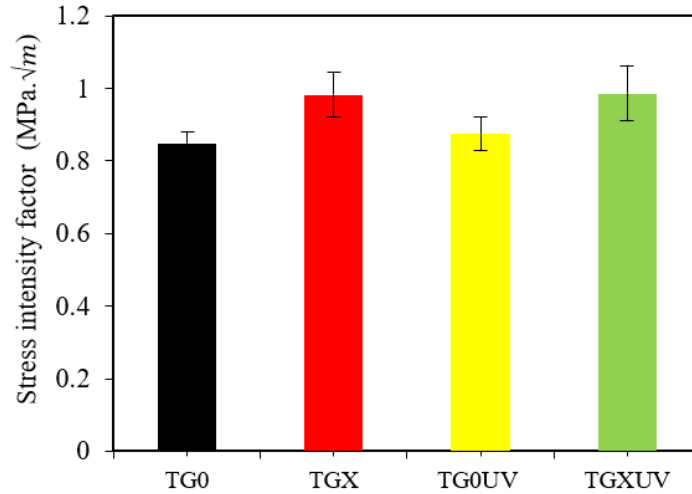


Figure 5. Stress intensity factor values of the SENB specimens

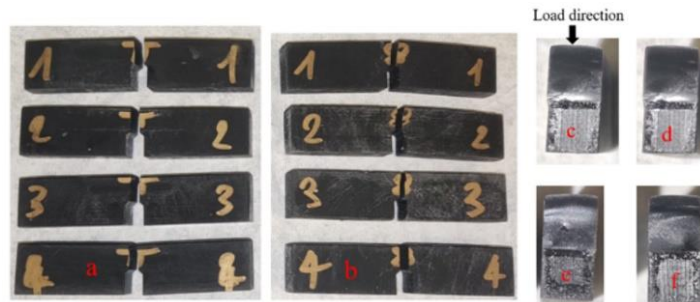


Figure 6. Failed SENB specimens (a) TGX, (b) TGX-UV, (c) TG0, (d) TGX, (e) TG0-UV and (f) TGX-UV

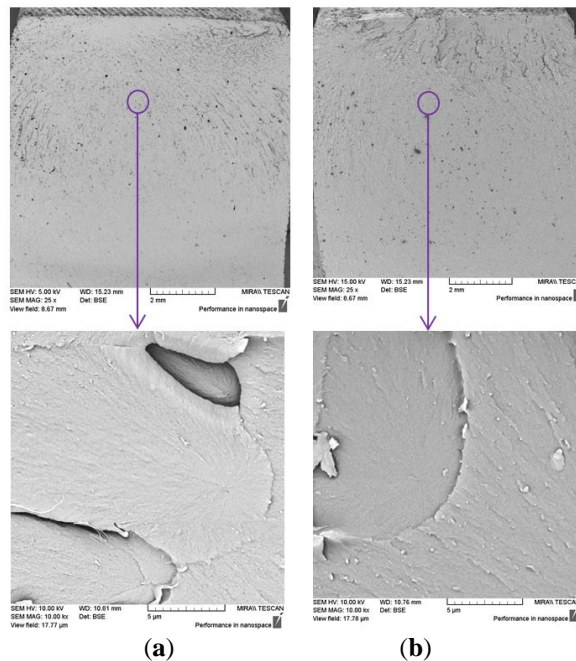


Figure 7. SEM of the (a) TG0 and (b) TGX of the failed SENB specimens

Thermal and Chemical Behaviour

The DSC test was carried out to present the amorphous nature and crosslinking level of the 3DPd components. Figure 8a displays the DSC heating and cooling curves for the TG0, TGX, TG0UV and TGXUV samples before and after AWRTH of 1000 hrs. The variations of heat flow (exotherm and endotherm) obtained from the DSC test as a function of temperature indicated that the 3DPd samples were highly crosslinked amorphous nature that didn't observe the endothermic peak of crystal performance or crystalline domains. Additionally, the curing process didn't affect after the addition of mGNP. On the other hand, after AWRTH ageing the heat flow of the 3DPd samples heating up to 225 °C and cooling to 0 °C was stable behaviour.

The FTIR test was conducted to investigate the alterations in the chemical bonds due to outdoor accelerated weathering of TG0 and TGX samples (Figure 8b). The ester bonds represented by C–O stretching were located from 1000 cm^{-1} to 1300 cm^{-1} . When the samples are under AWRTH exposure, photo-cleavage of ester bonds can occur (Barkane et al., 2023; Shanti et al., 2017). At the same time, the bonds of C=C stretching may be used to generate crosslinking to form oligomers or add chain length to the existing network. These bonds may appear due to limitations of crosslinking conversion during the resin photopolymerisation (Barkane et al., 2022, 2023). The peaks at 2863 cm^{-1} and 2940 cm^{-1} can be ascribed to the symmetric stretching of CH_2 and CH_3 , respectively (Wu et al., 2019). The AWRTH led to increased peak intensities of 1630 cm^{-1} and 2940 cm^{-1} for the C=C stretching and CH_2/CH_3 , respectively. On the other hand, the mGNP appeared at the peak bonds of C–O stretching and wasn't affected by AWRTH.

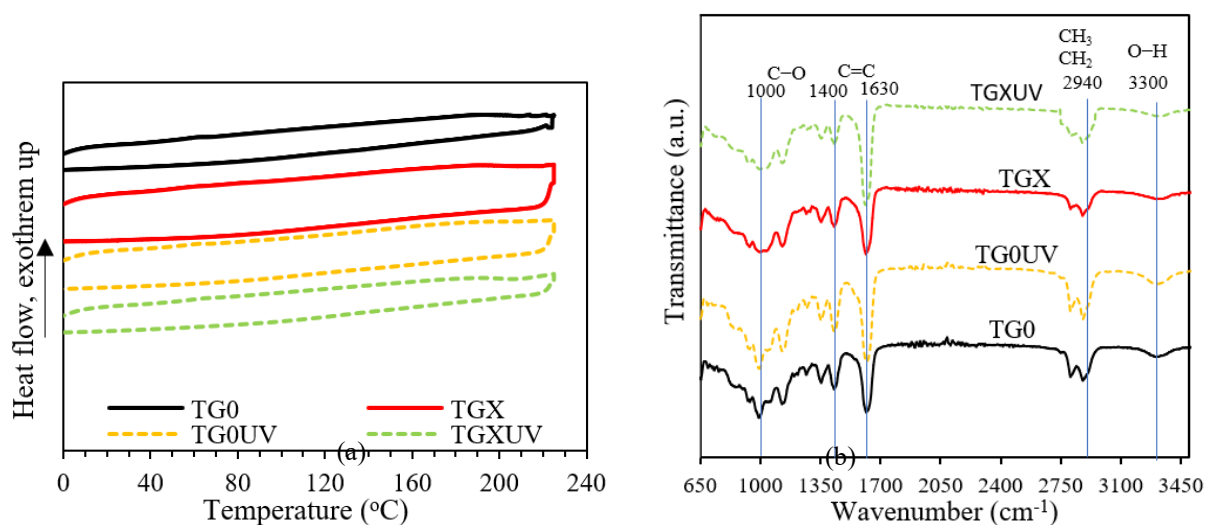


Figure 8. Thermal and chemical behaviour (a) DSC analysis and ; (b) FTIR spectra.

Shape-Memory Behaviour

The SM performance of the 3DPd specimens undergoing repeated thermomechanical cycles is illustrated in the 3D diagram as shown in Figure 9. Table 1 shows the average results of the maximum strain, fixity strain, and residual strain as obtained from the DMA machine, while the values of recovery ratio and fixity ratio were calculated by equations 1 and 2 in section 2.2. As shown in this figure, after releasing the force at a low temperature (-10 °C) and heating the sample inside the DMA machine the strain didn't decrease until the temperature reached the lower T_g (taken from the loss modulus). In other words, for all curves when heating the samples the recovery stage starts when the 3DPd sample enters the transition region between the glassy and rubbery behaviour and it is around 50 °C. Hence, molecular chain mobility becomes easier at the glass transition region. Hence, the fixity strain, ϵ_f , of (11.06, 10.29, 10.07, and 9.72) for the TG0, TGX, TG0UV and TGXUV samples with a maximum R_f of 97.7% was obtained for the unmodified resin. It is worth noticing that the sample recovered most of its original shape gradually at the glass transition region showing residual strain, ϵ_r , of (11.32, 10.58, 10.28, and 9.85) for the TG0, TGX, TG0UV and TGXUV samples with a maximum R_r of 94.1% obtained with including functionalised graphene nanoplatelets. All the R_r values were above 90 with a slight increase including mGNP and after the accelerating aging. This developed novel SMP can expand the 4DPg technology in industrial applications such as soft robotics as actuators and thermal sensors.

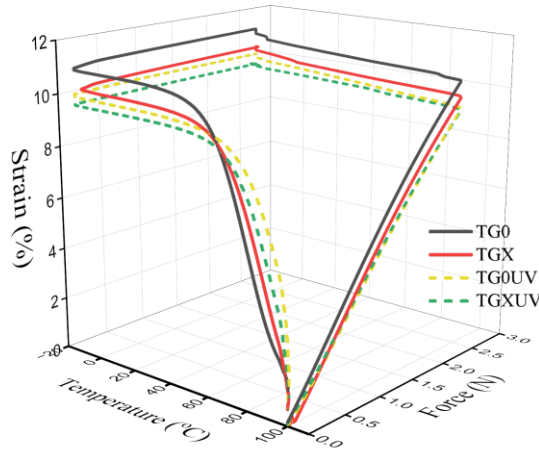


Figure 9. SM behaviour of 3DPd samples from the 4-steps-DMA thermomechanical cyclic test.

Table 1. Strain, recovery, and fixity ratios obtained from the 4-steps-DMA thermomechanical cyclic test.

| Property (%) | TG0 | TGX | TG0-UV | TGX-UV |
|--------------|-------|-------|--------|--------|
| ϵ_m | 11.32 | 10.58 | 10.28 | 9.85 |
| ϵ_f | 11.06 | 10.29 | 10.07 | 9.72 |
| R_f | 97.7 | 97.2 | 97.9 | 98.6 |
| ϵ_r | 1.13 | 0.62 | 0.64 | 0.69 |
| R_r | 90.2 | 94.1 | 93.7 | 92.9 |

Conclusion

In this work, a Figure 4[®] DLP UV-based 3D printer has been utilized to produce 4DPd polymeric-based structures. This study aims to focus on developing 3DPg of a commercial methacrylate-based resin by incorporating modified GNP with melamine to investigate the thermal and SM behaviour of 4DPd weather-resistant objects. The results showed good resistance to 1000 hrs weathering ageing and enhancement by incorporating functionalised graphene nanoplatelets. The maximum increment values of the tensile strength, impact resistance and critical stress intensity factor were 18%, 25% and 16%, respectively. The glass transition temperature values were slightly increased. The shape fixity ratios and the shape recovery ratios were greater than 97% and 90%, respectively. The results clarified that the heat flow variations (exotherm and endotherm) obtained from the DSC tests indicated that the 3DPd samples were fully cured after the UV printing process and UV post-cure. FTIR results showed a slight alteration of increasing in the peak intensities of the chemical bonds due to outdoor accelerated weathering and mGNP. The TG0, TGX, TG0UV and TGXUV of the 3DPd samples exhibited shape fixity ratios and shape recovery ratios greater than 97% and 90%, respectively. This study aims to provide knowledge in developing and expanding 4DPd objects for different engineering applications. Hence, the developed 3DPd specimens exhibited extraordinary durability for several SM cycle-life with the effect of mGNP and AWRTH. Finally, future research will have the opportunity to study how various accelerating weathering ageing conditions, and different mGNP contents and compositions affect various properties of 3DPd components, aiming to improve the longevity and durability of 3DPd materials.

Scientific Ethics Declaration

The authors declare that the scientific ethical and legal responsibility of this article published in EPSTEM journal belongs to the authors.

Acknowledgements or Notes

* This article was presented as an oral presentation at the International Conference on Basic Sciences, Engineering and Technology (www.icbasaset.net) held in Alanya/Turkey on May 02-05, 2024.

* The authors would like to express their sincere appreciation to the expert engineers Alexandre Portela and Tielidy A. de M. de Lima, PRISM Research Institute, Technological University of the Shannon, for their support in conducting the DMA, DSC and FTIR tests. The authors would like to extend gratitude to leading engineer James Wall for utilising the resin Tough Blk-20 and Figure® 4 DLP printer at 3D Technology Ltd company, Galway, Ireland.

* This research project is funded by Marie Skłodowska-Curie grant agreement No. 847577 cofounded by the European Regional Development Fund and Science Foundation Ireland (SFI) under Grant Number SFI/16/RC/3918 (Smart Manufacturing, Confirm Centre, UL).

References

- Afshar, A., Liao, H.-T., Chiang, F., & Korach, C. S. (2016). Time-dependent changes in mechanical properties of carbon fiber vinyl ester composites exposed to marine environments. *Composite Structures*, *144*, 80–85.
- Afshar, A., Mihut, D., Baqersad, J., & Hill, S. (2019). Study of metallic thin films on epoxy matrix as protective barrier to ultraviolet radiation. *Surface and Coatings Technology*, *367*, 41–48.
- Afshar, A., & Wood, R. (2020). Development of weather-resistant 3D printed structures by multi-material additive manufacturing. *Journal of Composites Science*, *4*(3), 94.
- Alfaro, M. E. C., Stares, S. L., Barra, G. M. de O., & Hotza, D. (2022). Effects of accelerated weathering on properties of 3D-printed PLA scaffolds. *Materials Today Communications*, *33*, 104821.
- Alsaadi, M., Hinchy, E. P., McCarthy, C. T., Moritz, V. F., Portela, A., & Devine, D. M. (2023). Investigation of thermal, mechanical and shape memory properties of 3D-printed functionally graded nanocomposite materials. *Nanomaterials*, *13*(19), 2658.
- Alsaadi, M., Hinchy, E. P., McCarthy, C. T., Moritz, V. F., Zhuo, S., Fuenmayor, E., & Devine, D. M. (2023). Liquid-based 4d printing of shape memory nanocomposites: A review. *Journal of Manufacturing and Materials Processing*, *7*(1), 35.
- Barkane, A., Jurinovs, M., Briede, S., Platnieks, O., Onufrijevs, P., Zelca, Z., & Gaidukovs, S. (2022). Biobased resin for sustainable stereolithography: 3D printed vegetable oil acrylate reinforced with ultra-low content of nanocellulose for fossil resin substitution. *3D Printing and Additive Manufacturing*.
- Barkane, A., Platnieks, O., Vecstaudza, J., & Gaidukovs, S. (2023). Analysis of bio-based acrylate accelerated weathering: A study of nanocellulose impact on the bulk durability of 3D-printed nanocomposites. *Materials Today Chemistry*, *33*, 101737.
- Bass, L., Meisel, N. A., & Williams, C. B. (2016). Exploring variability of orientation and aging effects in material properties of multi-material jetting parts. *Rapid Prototyping Journal*, *22*(5), 826–834.
- Cha, J., Kim, J., Ryu, S., & Hong, S. H. (2019). Comparison to mechanical properties of epoxy nanocomposites reinforced by functionalized carbon nanotubes and graphene nanoplatelets. *Composites Part B: Engineering*, *162*, 283–288.
- Chowdhury, J., Anirudh, P. V., Karunakaran, C., Rajmohan, V., Mathew, A. T., Koziol, K., Alsanie, W. F., Kannan, C., Balan, A. S. S., & Thakur, V. K. (2021). 4D printing of smart polymer nanocomposites: integrating graphene and acrylate based shape memory polymers. *Polymers*, *13*(21), 3660.
- Golhin, A. P., Srivastava, C., Strandlie, A., Sole, A. S., & Grammatikos, S. (2023). Effects of accelerated aging on the appearance and mechanical performance of materials jetting products. *Materials & Design*, *228*, 111863.
- Heravi, M. M., Ghavidel, M., & Mohammadkhani, L. (2018). Beyond a solvent: triple roles of dimethylformamide in organic chemistry. *RSC Advances*, *8*(49), 27832–27862.
- Mahmood, A., Akram, T., Shenggui, C., & Chen, H. (2023). Revolutionizing manufacturing: A review of 4D printing materials, stimuli, and cutting-edge applications. *Composites Part B: Engineering*, *266*, 110952.
- Mao, Y., Yu, K., Isakov, M. S., Wu, J., Dunn, M. L., & Jerry Qi, H. (2015). Sequential self-folding structures by 3D printed digital shape memory polymers. *Scientific Reports*, *5*(1), 13616.
- Pisani, S., Genta, I., Modena, T., Dorati, R., Benazzo, M., & Conti, B. (2022). Shape-memory polymers hallmarks and their biomedical applications in the form of nanofibers. *International Journal of Molecular Sciences*, *23*(3), 1290.
- Prashar, G., Vasudev, H., & Bhuddhi, D. (2022). Additive manufacturing: Expanding 3D printing horizon in industry 4.0. *International Journal on Interactive Design and Manufacturing (IJIDeM)*, *17*(5), 2221–2235.
- Shanti, R., Hadi, A. N., Salim, Y. S., Chee, S. Y., Ramesh, S., & Ramesh, K. (2017). Degradation of ultra-high molecular weight poly(methyl methacrylate-co-butyl acrylate-co-acrylic acid) under ultra violet irradiation. *RSC Advances*, *7*(1), 112–120.
- Shen, X., Wang, Z., Wu, Y., Liu, X., & Kim, J.-K. (2016). Effect of functionalization on thermal conductivities

- of graphene/epoxy composites. *Carbon*, 108, 412–422.
- Spiridon, I., Darie-Nita, R. N., & Bele, A. (2018). New opportunities to valorize biomass wastes into green materials. II. Behaviour to accelerated weathering. *Journal of Cleaner Production*, 172, 2567–2575.
- Vatanparast, S., Boschetto, A., Bottini, L., & Gaudenzi, P. (2023). New trends in 4D printing: A critical review. *Applied Sciences*, 13(13), 7744.
- Wu, H., Chen, P., Yan, C., Cai, C., & Shi, Y. (2019). Four-dimensional printing of a novel acrylate-based shape memory polymer using digital light processing. *Materials & Design*, 171, 107704.
- Wu, H., Fahy, W. P., Kim, S., Kim, H., Zhao, N., Pilato, L., Kafi, A., Bateman, S., & Koo, J. H. (2020). Recent developments in polymers/polymer nanocomposites for additive manufacturing. *Progress in Materials Science*, 111(1), 100638.
- Yu, K., Ritchie, A., Mao, Y., Dunn, M. L., & Qi, H. J. (2015). Controlled sequential shape changing Components by 3D Printing of Shape Memory Polymer Multimaterials. *Procedia IUTAM*, 12, 193–203.
- 3D Systems Inc. (n.d.). *Figure 4 tough-blk 20*. Retrieved from <https://www.3dsystems.com/materials/figure-4-tough-blk-20>

Author Information

Mohamad Alsaadi

CONFIRM Centre for Smart Manufacturing, University of Limerick, Limerick, Ireland
Technological University of the Shannon, Athlone, Ireland
Contact e-mail: mohamad.alsaadi@ul.ie

Eoin P. Hinchy

School of Engineering, University of Limerick
Limerick, Ireland

Conor T. McCarthy

School of Engineering, University of Limerick
Limerick, Ireland

Declan M. Devine

PRISM Research Institute, Technological University of the Shannon
Athlone, Ireland

To cite this article:

Alsaadi, M., Hinchy, E.P., McCarthy, C. T., & Devine, D. M. (2024). Effect of graphene nanoplatelets and accelerated weathering on the mechanical and shape memory behaviour of 3D printed components. *The Eurasia Proceedings of Science, Technology, Engineering & Mathematics (EPSTEM)*, 28, 47-55.